Acta of Bioengineering and Biomechanics
Vol. 24, No. 3, 2022

Original paper
DOI: 10.37190/ABB-02154-2022-02

Some aspects related to the indentation-based viscoelastic modelling of trabecular bone tissue

KRZYSZTOF JANKOWSKI*, MAREK PAWLIKOWSKI, KATARZYNA BARCZ

Institute of Mechanics and Printing, Warsaw University of Technology, Warszawa, Poland.

Purpose: The aim of this research was to verify to what extent the shape of an indenter tip influences the final form of the constitutive equation for the trabecular bone. *Methods*: Trabecular bone was formulated as a non-linear viscoelastic material with Mooney–Rivlin hyperelastic model to describe the purely elastic response of the bone tissue. Tests of the mechanical properties of the trabecular bone, resected from the femoral head of a 56-year-old patient, were carried out with two types of indenter: the spherical tip of a diameter of 200 μm and pyramid Vickers tip with 136° between plane faces. Tests with both indenters included loading and unloading phases with no hold at peak force and with hold time t = 20 s and were conducted with a maximum load P_{max} = 500 mN and loading/unloading rate V = 500 mN/min. *Results*: The formulated constitutive model describes the trabecula behaviour very well. The model curves match the experimental results in the loading phase, holding period and most of the unloading ramp. The purely viscoelastic material constants are very close in value for both considered tips, but purely elastic constants differ. *Conclusions*: The results indicate that the constitutive model based on the indentation with the Vickers tip does not cover the plastic residual deformation. When a viscoelastic response of bone is expected, a model with constants calibrated for the spherical tip should be used, and the other set of parameters values (Vickers tip) when trabeculae may undergo plastic deformation.

Key words: *constitutive model, non-linear viscoelasticity, trabecular bone, indentation, finite element method*

1. Introduction

Bone properties have been studied by means of various experimental methods [2], [3], [14], [15], [35]. One of the most popular experimental procedures is the indentation technique which has been successfully utilised in bone tissue properties research. The indentation tests can be carried out on both micro- and macro-scales. The multi-scale approach in bone properties research is very beneficial as it enables us to draw information on the hierarchical structure of the tissue. One of the first attempts to formulate a multi-scale model of bone is presented in [28]. The author proposed a model to predict the influence of mineral volume fraction and particle aspect ratio on the elastic modulus of bone. The bone was considered as a mineralised polymer composite with high aspect ratio filler particles. Although it was formulated for cortical tissue, the author claims that the model can be extended to include the effect of porosity in trabecular bone. In 2009, Ghanbari and Naghdabadi proposed a hierarchical multi-scale model for cortical bone [6]. They presented a model which predicts the mechanical properties of the tissue, such as the Young's modulus, shear modulus and Poisson's ratio. They used a homogenisation scheme to calculate macroscopic stress from stress distribution on the microscale and transfer it back to the macroscale. The authors concluded that their method could be used to determine the mechanical properties of cortical bone. Jaziri et al. [12] developed a model for bovine trabecular bone describing the elastoplastic behaviour of the tissue under compression loading. They used a homogenisation method to define the elastic properties of the bone and proposed a constitutive plastic-damage model to describe

* Corresponding author: Krzysztof Jankowski, Institute of Mechanics and Printing, Warsaw University of Technology, ul. Narbutta 85, 02-524 Warszawa, Poland, e-mail: krzysztof.jankowski.wip@pw.edu.pl
Received: November 14th, 2022
Accepted for publication: January 17th, 2023

its response. A homogenisation approach is also presented in [34] to evaluate the influence of resorption cavities on the mechanical properties of cortical bone and by Atthapreyangkul et al. [1], who performed multi-scale finite element analysis to determine the effect of geometrical changes at multiple structural scales on the mechanical properties of cortical bone. Rahmoun et al. [29] proposed a micromechanical formula to model the elastic response of the human humerus. The authors coupled a two-phase micromechanical approach by using a homogenisation scheme for cylindrical voids in the bone and nanoindentation measurements to determine the elastic modulus of the bone matrix phase.

The indentation tests consist in emerging a tip of a particular size and geometry into a studied material. In the case of indentation tests on bone samples, the tip geometry determines the effects that are revealed in the tissue during the experiments. Not only can the data obtained from the experimental tests be utilised to determine the basic mechanical properties of bone, but it can also be employed to formulate a constitutive equation for bone tissue behaviour. Various constitutive models have been proposed so far. They differ from each other by the effects they consider and by the experimental protocol they are based on. As for the effects, visco-elasto-plasticity of bone can be addressed [19], as well as viscoplasticity [13], damage propagation [5] or non-linear viscoelasticity [25]. The models are usually based on compression tests conducted at various strain rates. A non-linear viscoelastic constitutive model based on indentation tests results was proposed in [26]. The tests were conducted with a spherical tip without a hold phase in the force history.

In constitutive formulation based on indentation experiments, usually the Oliver–Pharr theory [21] is considered to propose a constitutive model. However, such an approach cannot be undertaken in the case of materials indicating viscoelastic or visco-plastic effects [20], [22]. One of the ways to cope with the problem is to formulate a model based on mechanical elements [23]. Such constitutive models, however, describe the studied material in a linear domain. Moreover, in the case of indentation, a model in the force-depth (P–h) domain is usually formulated. Both those factors make the approach unhelpful to constitutively describe bone, as the tissue indicates non-linear effects.

In the present paper, we propose a formulation of a non-linear viscoelastic constitutive model in the stress-strain domain based on indentation tests, which were conducted with two different tips, i.e., a spherical tip and a Vickers tip. The former one is a rounded indenter, while the latter one is a sharp tip. The objective of the research is to verify to what extent the shape of an indenter tip influences the final form of the constitutive equation for trabecular bone. Since mechanical properties determined based on indentation tests with rounded and sharp tips differ, we thus expect to obtain different values of the material parameters in the constitutive model for the two tips. One of the previous studies [26] showed that a spherical indenter is adequate to formulate a viscoelastic constitutive model for bone tissue. Thus, the criterium of our thesis verification is a comparison of the model parameters values identified from the curve-fitting of the model curves and those obtained from the experiments conducted with the two indenters.

2. Materials and methods

2.1. Preparation of trabecular bone sample

The human trabecular bone specimen was resected from the femoral head of a 56-year-old patient during a hip replacement surgery after approval of the Bioethics Committee of Military Medicine Institute in Warsaw, Poland. The patient was a female who suffered from arthritis. The cube bone sample with dimensions of 15 × 15 × 15 mm was cut out from the specimen with a saw blade according to the arrangement of the trabeculae. Cutting directions were selected in relation to the geometrical features of the bone. The following parameters of the cutting process were applied: i) saw blade shaft speed n = 3300 rpm, ii) saw blade feed f = 0.17 mm/rev, iii) blade appropriate to cut materials of hardness 70 – 400 HV. The marrow was removed after cutting. The sample was stored in 95% ethanol at a temperature of 4 °C for several hours [4], [17].

2.2. Microindentation tests

The studies of mechanical properties of trabecular bone were carried out on the CSM Microhardness Tester with two types of an indenter: the diamond spherical tip of a diameter of 200 μm and pyramid Vickers tip with 136° between plane faces. Tests with both indenters were conducted with a value of maximum load P_{max} = 500 mN and with loading/unloading rate V = 500 mN/min. Tests included loading and

unloading phases with no hold at peak force and with hold time t = 20 s. The measured force P as a function of microindentation depth h made it possible to obtain hysteresis loops. Young's modulus was directly calculated during measurements from indentation curves by the Oliver–Pharr method [21]. The value of the trabecular bone Poisson ratio ν was set at 0.3 [30].

The bone sample was drained from ethanol in a controlled environment (temperature of 20° ± 5° and humidity 32% ± 5%) for an hour before the tests. The region of interest during indentations was selected arbitrarily. Four trabeculae were chosen randomly. Three microindentations on the same trabecula were performed within each set of test parameters, giving 12 measurements. Because the mechanical properties of the core and the side surface of the trabecular bone differ [9], [37], which is connected to the different mineralization levels [16], indentations were made randomly in both areas.

2.3. The constitutive model

Trabecular bone was considered as a non-linear viscoelastic material. In non-linear viscoelasticity, the constitutive equation is formulated as a convolution of strain-dependent $\mathbf{S}^{\mathbf{S}}(\lambda)$ and a time-dependent function $g(t)$:

$$\mathbf{S}(\lambda, t) = \mathbf{S}^{\mathbf{S}}(\lambda) * g(t), \tag{1}$$

where: $\mathbf{S}$ – second Piola–Kirchhoff stress tensor, $\mathbf{S}^{\mathbf{S}}$ – elastic second Piola–Kirchhoff stress tensor, λ is stretch ratio along the loading direction, t represents time. Equation (1) can be written as:

$$\mathbf{S}(t) = g_{\infty}\mathbf{S}^{\mathbf{S}}(t) + \sum_{i=1}^{n}\int_{0}^{t} g_i \cdot e^{\frac{t-s}{\tau_i}} \frac{\partial \mathbf{S}^{\mathbf{S}}(s)}{\partial s} ds, \tag{2}$$

after splitting into elastic and viscoelastic terms using Prony series:

$$g(t) = g_{\infty} + \sum_{i=1}^{n} g_i \cdot e^{\frac{t}{\tau_i}}, \tag{3}$$

where: τ_i – relaxation times, g_i – viscoelastic constants, n – indicates a number of relaxation times τ_i and viscoelastic constants g_i (i = 1, ..., n),

$$g_{\infty} = 1 - \sum_{i=1}^{n} g_i . \tag{4}$$

The variable s in Eq. (2) represents the historical time. To calculate $\mathbf{S}(t)$ the strain history has to be known. Relaxation times and viscoelastic constants are identified using data from experiments.

The elastic part of the second Piola–Kirchhoff stress is calculated using of Eq. (5):

$$S_{ij}^{s} = \frac{2\partial \Psi}{\partial C_{ij}}, \tag{5}$$

where: C_{ij} (i, j = 1, 2, 3) are components of the right Cauchy deformation tensor $\mathbf{C}$.

We propose the two-parameter Mooney–Rivlin hyperelastic model to describe the purely elastic response of the bone tissue. Therefore, the strain energy function Ψ in (5) takes the form [18]:

$$\Psi = c_{10}(I_1 - 3) + c_{01}(I_2 - 3), \tag{6}$$

where: I_1 and I_2 are the first and second invariants of tensor $\mathbf{C}$, c_{10} and c_{01} are hyperelastic constants, which are also identified using data from experiments. The bone is treated as an incompressible material. More details are described in the paper [11].

By means of algorithm used in [7], stress in Eq. (2) can be computed using the formula:

$$\mathbf{S}(t+1) = g_{\infty}\mathbf{S}^{\mathbf{S}}(t+1) + \sum_{i=1}^{n}\left(e^{\frac{-\Delta t}{\tau_i}} \cdot \mathbf{Q}_i(t) + g_i \frac{1 - e^{\frac{-\Delta t}{\tau_i}}}{\frac{\Delta t}{\tau_i}} (\mathbf{S}^{\mathbf{S}}(t+1) - \mathbf{S}^{\mathbf{S}}(t)) \right). \tag{7}$$

In Equation (7), Δt represents the time increment, $\mathbf{Q}_i(t)$ is the stress at the previous time step. Because initial stress and strain in the material are known, the stress at time $t > 0$ can be calculated.

2.4. The constants identification

The process of constants identification was split into two stages. In the first stage, the number n and values of relaxation times τ_i (i = 1, ..., n) were determined using data from the stress relaxation test performed on the cuboid sample. The algorithm of identification is based on iterative calibration and is described in detail in [23]. The stress relaxation test was conducted on MTS Bionix Systems on the cuboid bone sample. The bone sample was drained for an hour at room temperature before the test. During the experiment, the sample was compressed to the strain value of 0.01 within 160 s. The stress relaxation was registered for 500 s. The relaxation times τ_i were calibrated by fitting the curve described by Eq. (7) to the

relaxation part of the curve obtained from the experiment. The identification was conducted in Matlab using our script.

In the second stage, the hyperelastic constants c_{10} and c_{01}, as well as viscoelastic constants g_i (i = 1, ..., n), were calibrated using an indirect method based on finite element (FE) analyses. These constants were calibrated by fitting the curves obtained from the FE simulations of microindentation, which we performed in ANSYS Workbench 2021 R1, to the corresponding experimental curves. To complete the task, the constitutive equation was implemented into ANSYS Workbench 2021 R1 using two material model options, i.e., the Mooney–Rivlin hyperelastic model (purely elastic response) and Prony Shear Relaxation series (viscoelastic properties). The equation was implemented with the initial values of the parameters. After running the simulations, the results in the form of the P–h curves were compared to those obtained in the experiments. If the curves from the simulations did not match the experimental ones, the next simulation with new values of the parameters was conducted. The procedure was repeated until satisfactory values of errors were obtained. The criteria of the procedure ending are presented in Section 3.

In the three-dimensional simulations of microindentation, indenters were modelled as an elastic material (the Young's modulus $2 \cdot 10^5$ MPa, the Poisson ratio 0.3), and trabecula was modelled by means of the formulated constitutive equation. Models of trabecula and indenters were designed in SolidWorks, saved as a STEP file, and imported into ANSYS. The spherical indenter was modelled as half of the sphere with a diameter of 200 μm and the Vickers indenter as a pyramid with a base size of 40 μm. The model of trabecular bone for simulation with spherical tip was modelled as a cuboid with dimensions 340 × 340 × 120 μm, and for Vickers as a cuboid with dimensions 120 × 120 × 60 μm. In ANSYS, the model of the spherical indenter was meshed with tetrahedron elements with a dimension of 20 μm and for Vickers indenter with a dimension of 6 μm, while the models of trabecular bone were meshed with hexahedron elements with two different sizes: 7 μm near the area of contact and 15 μm in the rest part of the model for simulation with the spherical indenter (Fig. 1a) and 2 μm near the area of contact and 6 μm in the rest part of the model for simulation with the Vickers indenter (Fig. 1c). The mesh study was conducted to find the optimal mesh density. Bone models were fixed on the bottom surface. Contact between models of trabecular bone and indenter was set as frictionless. The force was applied to the top surface of the indenters. In simulations, the whole load and unload cycle was considered with the same parameters as in the experiment. It gave a total number of 12 unique simulations, the same amount as microindentations.

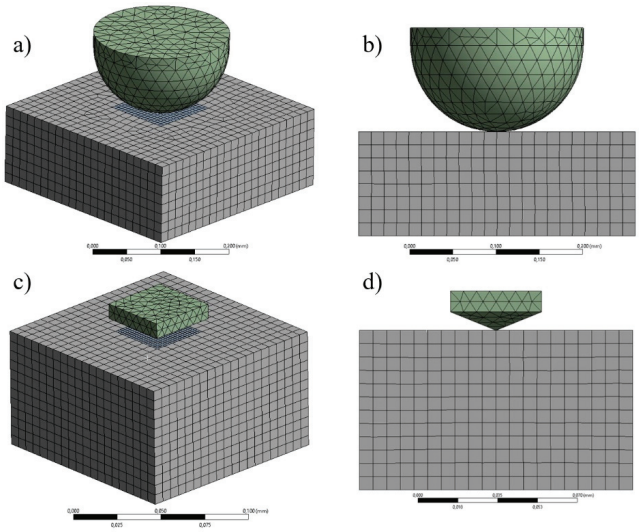

Fig. 1. Meshed models of indenter and trabecula: a) spherical indenter in isometric view, b) spherical indenter in front view, c) Vickers indenter in isometric view, d) Vickers indenter in front view

3. Results

3.1. Identification of relaxation times

The algorithm described in [24], which was applied during the process of fitting the curve defined by the formulated constitutive model to the curve from the experiment of the stress relaxation, gave a result regarding the number of relaxation times n and the values of relaxation times τ_i. It appeared that four re-

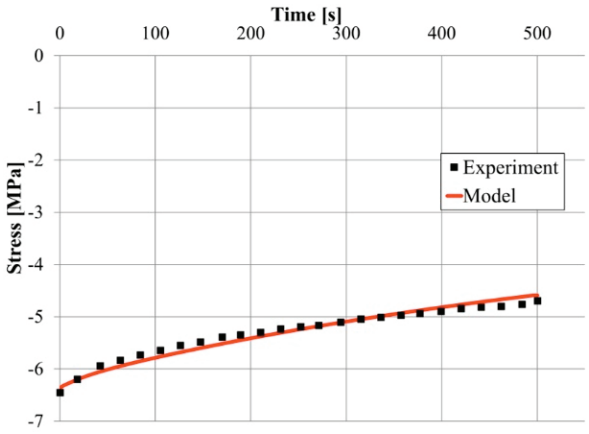

Fig. 2. Model curve fitted to the stress relaxation test results

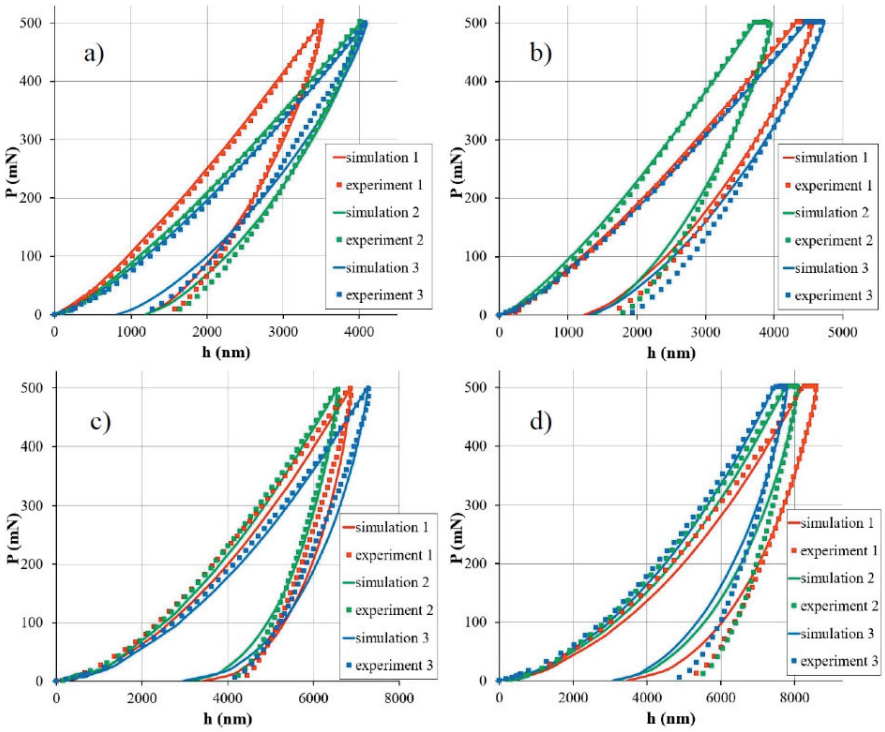

Fig. 3. Curves from simulations fitted to the microindentation results for:
a) spherical indenter t = 0 s, b) spherical indenter t = 20 s, c) Vickers indenter t = 0s, d) Vickers indenter t = 20 s

laxation times were enough to describe the viscoelastic behaviour of the trabecular bone. It means that n in Eq. (2) is equal to 4. The result of the curve-fitting process is shown in Fig. 2. The curve obtained from the experiment is represented by squares, while the curve described by Eq. (7) is represented by a solid line. The identified values of the relaxation times are: τ_1 = 1 s, τ_2 = 8 s, τ_3 = 63 s, τ_4 = 500 s. The relaxation times determine how quickly the material recovers from the applied load.

In Figure 3, graphical representation of microindentation curve-fitting process is presented. Curves from the experiments are shown by means of squares, while curves described by the constitutive model and obtained from the simulations are represented by a solid line.

3.2. Identification of hyperelastic and viscoelastic constants

In the curve-fitting process, four criteria of fit were established. Three of them were connected with the comparison of the areas obtained from experiment A_{exp} and simulation A_{sim} and were as follows: the error of fitting the areas under the loading part of the curves had to be under 10%, the error of fitting the areas of hysteresis loops had to be under 10%, and error of fitting the areas under the unloading part of the curves had to under 15%. The areas were calculated numerically from force-displacement curves using a trapezoidal integration rule. The areas-fitting errors were determined using the following formula:

$$\text{err} = \left| \frac{A_{sim} - A_{\text{exp}}}{A_{\text{exp}}} \right| \cdot 100\% \,. \tag{8}$$

The values of the error are presented in Tables 1–3.

Table 1. Values of areas-fitting error of loading part of the curves

Indenter	Pause [s]	Areas-fitting error [%]		
		Simulation 1	Simulation 2	Simulation 3
Spherical	0	3.43	2.97	2.87
	20	3.97	4.31	0.84
Vickers	0	8.25	4.67	3.72
	20	5.76	5.39	3.10

Table 2. Values of areas-fitting error of hysteresis loops

Indenter	Pause [s]	Areas-fitting error [%]		
		Simulation 1	Simulation 2	Simulation 3
Spherical	0	2.90	0.59	5.76
	20	3.11	3.92	9.45
Vickers	0	4.98	6.97	1.03
	20	16.02	26.17	20.61

Table 3. Values of areas-fitting error of unloading part of the curves

Indenter	Pause [s]	Areas-fitting error [%]		
		Simulation 1	Simulation 2	Simulation 3
Spherical	0	3.92	4.85	1.60
	20	9.73	14.06	11.36
Vickers	0	13.77	0.72	6.99
	20	10.71	38.71	30.51

The fourth criterion was the error of position of the curves' peaks from experiment h_{exp} and simulation h_{sim} which had to be under 1%. In this criterion, only the maximum depth of microindentation from the experiment and simulation was considered because the maximum load in the experiment and in the corresponding simulation was the same. The error was determined using the formula:

$$\text{err} = \left| \frac{h_{sim} - h_{\text{exp}}}{h_{\text{exp}}} \right| \cdot 100\% \,. \tag{9}$$

The values of the error are presented in Table 4.

Table 4. Values of error of position of the curves' peaks

Indenter	Pause [s]	Error of position of the curves' peaks [%]		
		Simulation 1	Simulation 2	Simulation 3
Spherical	0	0.13	0.41	0.61
	20	0.69	0.14	0.03
Vickers	0	0.11	0.41	0.30
	20	0.77	0.70	0.72

Using the Mooney–Rivlin hyperelastic strain energy function enables to calculated values of Young Modulus E by means of the formula:

$$E = 2G(1+\nu)\,, \tag{10}$$

where: G is the Kirchhoff modulus and ν is a Poisson's ratio. The value of Poisson's ratio was the same as in the experiment, i.e., 0.3 while the Kirchhoff modulus was calculated using Eq. (11).

$$G = 2(c_{10} + c_{01})\,. \tag{11}$$

Table 5. Averaged values of elastic modulus measured in the experiments and predicted by the constitutive model

Indenter	Pause [s]	Young's modulus [GPa]		Mean error [%]
		Experiments	Model prediction	
Spherical	0	4.24 ± 0.92	4.99 ± 0.77	17.62
	20	3.62 ± 0.70	4.69 ± 0.81	29.83
Vickers	0	7.80 ± 1.69	5.58 ± 0.62	28.46
	20	6.55 ± 1.16	5.01 ± 0.81	23.57

Averaged values of the Young's modulus measured during experiments and calculated from simulation using Eq. (10) are shown in Table 5.

Identified during simulations hyperelastic and viscoelastic constants were averaged and are presented in Table 6. The constants were obtained from the FE simulation which gave the curves satisfying the above criteria. The constants c_{10} and c_{01} determined the elastic behaviour of trabecular bone while g_1, g_2, g_3, g_4 determined the width of the hysteresis loop and, with the relaxation times, the viscosity of the tissue.

Table 6. Averaged values of the identified material constants

Indenter	Spherical		Vickers	
Pause [s]	0	20	0	20
c_{10} [MPa]	3540 ± 149	3386 ± 119	2337 ± 148	1896 ± 249
c_{01} [MPa]	–2580 ± 45	–2483 ± 33	–1263 ± 52	–933 ± 125
g_1 [–]	0.12 ± 0.02	0.15 ± 0.01	0.1 ± 0.01	0.21 ± 0.01
g_2 [–]	0.19 ± 0.01	0.18 ± 0.02	0.1 ± 0.01	0.26 ± 0.03
g_3 [–]	0.27 ± 0.06	0.27 ± 0.02	0.55 ± 0.03	0.23 ± 0.04
g_4 [–]	0.05 ± 0.01	0.05 ± 0	0.05 ± 0	0.05 ± 0.01

4. Discussion

In the paper, we formulated a constitutive equation for trabecular bone based on microindentation experiments. The model was created on a microscopic scale, i.e., single trabeculae were indented. Thus, the material parameters we identified characterise the tissue from a microscale point of view.

In the experimental protocol, we used two types of indenters, i.e., a spherical one and a pyramidal one. The measurement data was utilised to identify the material parameters of our non-linear viscoelastic model, which we incorporated to describe mathematically trabecular bone on a microscale. Both purely elastic and viscoelastic constants were calibrated.

Time-dependent response of biological materials to mechanical loads, like creep or stress relaxation, is one of the major impediments to characterise the materials by means of indentation tests. However, as our objective was to formulate a non-linear viscoelastic constitutive model for the biological tissue, we were concerned to consider the time-dependent effects in our study. We did this twofold, i.e., by neglecting the time hold at peak load, and, to make the model more general, by applying a short (20 s) holding period. Usually, researchers design their experiment protocol such that the ramp load is followed by even 120 s

holding period to eliminate the time-dependent characteristics of bone response [40].

Analytically, the time-dependent effects are incorporated by combining formulae for elastic displacement with constitutive laws for the viscoelastic deformation of the tissue. This is realised by formulating hereditary convolution integrals over imposed strain history and material relaxation constants. Such an approach was incorporated in the present paper and has been developed for various types of tips, including spherical [31] and pyramidal ones [32]. The new aspect of the study shown in the paper consists of utilising the mentioned approach to formulate a constitutive equation for trabeculae and show the difference between the models based on spherical tip indentation and pyramidal tip indentation results.

In Figure 3, it was proved that the formulated constitutive model describes the trabecula behaviour very well. This is also presented in Tables 1, 2, and 4, where the curve fitting errors are depicted. The model curves match the experimental results in the loading phase, holding period and most of the unloading ramp. It can be seen that the residual depth predicted by our constitutive model is actually the same for the spherical indenter in comparison to the experimental depth. Conversely, it is lower in the case of the Vickers tip. This suggests that, firstly, the residual depth caused by the spherical tip is due to viscoelastic deformation of the trabecula, and, secondly, the constitutive model should be improved by an additional factor which will cover the part of the residual depth resulting from the viscoelastic and plastic strain caused by the Vickers embedding. The discrepancy in the model prediction of the spherical and pyramidal tips indentation can be seen in Tables 3 and 5, where the values of the errors of the unloading ramp fitting and the calculated Young's modulus are shown. The experimental Young's modulus was calculated directly from the measurement using Oliver–Pharr theory. The modulus values in the "Model prediction" column were calculated based on the Mooney–Rivlin coefficient values [27] presented in Table 6. It can be seen that although the predicted values of the Young's modulus obtained from the indentation of the two considered tips differ from each other, they are in the range of the modulus values obtained by other researchers [4], [10], [17], [37]. However, there are also studies that report higher values of the modulus [33], [39]. Those discrepancies result from the conditions of sample preparation or experimental test environment (wet vs. dry), the orientation of bone samples (transverse or longitudinal), age and the patients' health [38]. The error of the elastic modulus predicted by the model and that obtained from the measurements is relatively low, considering the fact that a biological tissue was studied. However, the error values are larger than in [11], where some measurements were also conducted with the spherical diamond tip with maximum load P_{max} = 500 mN and with loading/unloading rate V = 500 mN/min.

The values of the identified material constants are presented in Table 6. The purely elastic constants obtained from the spherical indentation differ from that resulting from the Vickers embedding. The maximal difference can be even 50%. This cannot be said about the purely viscoelastic constants, which are very close in value for both considered tips. This observation suggests that mainly the elastic response of the trabecula is affected by the tip geometry, whereas the viscoelastic behaviour seems to be described by the constitutive model equally well. However, it has to be noted that our model should be enriched by a plastic factor, which will allow us to predict also the plastic response of trabecula undergoing pyramidal tip indentation.

There are several limitations of our study. In terms of constitutive modelling, the limitations are:

1. one range of indentation force and one load rate were considered in the experimental protocol;
2. the stress–relaxation experiment was conducted on a cuboid sample of trabecular bone, thus, the determined values of relaxation times are proper for trabecular bone in general;
3. the proposed constitutive model can be utilised to numerically simulate trabecular bone in the range of viscoelastic deformation;
4. the model does not take plastic effects in bone into account.

Another limitation might be the fact that the bone samples were kept in alcohol. Such storage of biological tissues changes their mechanical properties. However, it has been proved that the type of medium in which bone samples are stored does not significantly influence bone properties in a small range of deformation [36]. Other authors reported some alterations in the mechanical properties of bone specimens during long-term immersion in alcohol [8]. In our studies, the time of the samples storage in ethanol was relatively short (hours rather than days), so its negative influence on the specimens' properties was minimised.

5. Conclusions

The proposed method of the constitutive model formulation can be successfully conducted using both spherical and Vickers tips. However, as it has been

agreed that a spherical indenter is adequate for bone indentation in the viscoelastic range of deformation, it seems that the pyramidal tip induces an additional effect in the trabeculae. This conclusion is based on the fact that the values of the viscoelastic constants are different for both indenters and in Fig. 3, where it can be seen that our model does not cover residual deformation resulting from plastic strain (Figs. 3c, d). An additional term responsible for plastic deformation in our model would probably amend the model prediction for the Vickers tip.

References

[1] ATTHAPREYANGKUL A., HOFFMAN M., PEARCE G., *Effect of geometrical structure variations on the viscoelastic and anisotropic behaviour of cortical bone using multi-scale finite element modelling*, J. Mech. Behav. Biomed. Mater., 2021, 113, 104153.

[2] BISWAS S., DASGUPTA P., PRAMANIK P., CHANDA A., *Macro and micro indentation behavior of the cortical part of human femur*, Procedia Materials Science, 2014, 5, 2320–2329.

[3] BÖHME B., LAURENT C., MILIS O., PONTHOT J.-P., BALLIGAND M., *Determination of Canine Long Bone Ultimate Tensile Strain by Digital Image Correlation*, J. Orthop. Res. Ther., 2022, 7, 1221, DOI: 10.29011/2575-8241.001221.

[4] CYGANIK Ł., BINKOWSKI M., KOKOT G., RUSIN T., POPIK P., BOLECHAŁA F., NOWAK R., WRÓBEL Z., JOHN A., *Prediction of Young's modulus of trabeculae in microscale using macroscale's relationships between bone density and mechanical properties*, J. Mech. Behav. Biomed. Mater., 2014, 36, 120–134.

[5] GARCIA D., ZYSSET P.K., CHARLEBOIS M., CURNIER A., *A three-dimensional elastic plastic damage constitutive law for bone tissue*, Biomech. Model Mechanobiol., 2009, 8, 149–165.

[6] GHANBARI J., NAGHDABADI R., *Nonlinear hierarchical multiscale modelling of cortical bone considering its nanoscale microstructure*, J. Biomech., 2009, 42, 1560–1565.

[7] GOH S.M., CHARALAMBIDES M.N., WILLIAMS J.G., *Determination of the constitutive constants of non-linear viscoelastic materials*, Mech. Time-Depend Mater., 2004, 8, 255–268.

[8] HAMMER N., VOIGT C., WERNER M., HOFFMANN F., BENTE K., KUNZE H., SCHOLZ R., STEINKE H., *Ethanol and formaldehyde fixation irreversibly alter bones' organic matrix*, J. Mech. Behav. Biomed. Mater., 2014, 29, 252–258.

[9] HARRISON N.M., MCDONNELL P.F., KENNEDY O.D., O'BRIEN F.J., MCHUGH P.E., *Heterogeneous linear elastic trabecular bone modelling using micro-CT attenuation data and experimentally measured heterogeneous tissue properties*, J. Biomech., 2008, 41 (11), 2589–2596.

[10] HONG J., CHA H., PARK Y., LEE S., KHANG G., KIM Y., *Elastic moduli and Poisson's ratios of microscopic human femoral trabeculae*, Proceedings of 11th Mediterranean Conference on Medical and Biomedical Engineering and Computing 2007, IFMBE16, 2007, 274–277.

[11] JANKOWSKI K., PAWLIKOWSKI M., DOMAŃSKI J., *Multi-scale constitutive model of human trabecular bone*, Continuum Mech. Thermodyn., 2022, DOI: doi.org/10.1007/s00161-022-01161-0.

[12] JAZIRI A., RAHMOUN J., NACEUR H., DRAZETIC P., MARKIEWICZ E., *Multi-scale modelling of the trabecular bone elastoplastic behaviour under compression loading*, Eur. Comput. Mech., 2012, 21, 254–269.

[13] JOHNSON T.P.M., SOCRATE S., BOYCE M.C., *A viscoelastic, viscoplastic model of cortical bone valid at low and high strain rates*, Acta Biomater., 2010, 6, 4073–4080.

[14] JONAS J., BURNS J., ABEL E.W., CRESSWELL M.J., STRAIN J.J., PATERSON C.R., *A technique for the tensile testing of demineralised bone*, J. Biomech., 1993, 26, 271–276.

[15] KLINGER S., GREINWALD M., AUGAT P., HOLLENSTEINER M., *Mechanical and morphometric characterization of custom-made trabecular bone surrogates*, J. Mech. Behav. Biomed. Mater., 2022, 129, 105146.

[16] LINDEN J.C., BIRKENHAGER-FRENKEL D.H., VERHAAR J.A.N., WEINANS H., *Trabecular bone's mechanical properties are affected by its non-uniform mineral distribution*, J. Biomech., 2001, 34, 1573–1580.

[17] MAKUCH A.M., SKALSKI K.R., *Human cancellous bone mechanical properties and penetrator geometry in nanoindentation tests*, Acta Bioeng. Biomech., 2018, 20 (3), 153–164.

[18] MOONEY M., *A theory of large elastic deformation*, J. Appl. Phys., 1940, 11, 582–592.

[19] NATALI A.N., CARNIEL E.L., PAVAN P.G., *Constitutive modelling of inelastic behaviour of cortical bone*, Med. Eng. Phys., 2008, 30, 905–912.

[20] OLESIAK S.E., OYEN M.L., FERGUSON V.L., *Viscous-elastic-plastic behavior of bone using Berkovich nanoindentation*, Mech. Time-Depend. Mater., 2010, 14, 111–124.

[21] OLIVER W.C., PHARR G.M., *An improved technique for determining hardness and elastic-modulus using load and displacement sensing indentation experiments*, J. Mater. Res., 1992, 7 (6), 1564–1583.

[22] OYEN M.L., *Sensitivity of polymer nanoindentation creep measurements to experimental variables*, Acta Mater., 2007, 55, 3633–3639.

[23] OYEN M.L., COOK R.F., *Load–displacement behavior during sharp indentation of viscous–elastic–plastic materials*, J. Mater. Res., 2003, 18, 139–150.

[24] PAWLIKOWSKI M., *Non-linear approach in visco-hyperelastic constitutive modelling of polyurethane nanocomposite*, Mech. Time-Depend. Mater., 2013, 18, 1–20.

[25] PAWLIKOWSKI M., BARCZ K., *Non-linear viscoelastic constitutive model for bovine cortical bone tissue*, Biocybern. Biomed. Eng., 2016, 36, 491–498.

[26] PAWLIKOWSKI M., JANKOWSKI K., SKALSKI K., *New microscale constitutive model of human trabecular bone based on depth sensing indentation technique*, J. Mech. Behav. Biomed. Mater., 2018, 85, 162–169.

[27] PAWLIKOWSKI M., SKALSKI K., SOWIŃSKI T., *Hyper-elastic modelling of intervertebral disc polyurethane implant*, Acta Bioeng. Biomech., 2013, 15, 43–50.

[28] PORTER D., *Pragmatic multiscalemodelling of bone as a natural hybrid nanocomposite*, Mater. Sci. Eng., 2004, A 365, 38–45.

[29] RAHMOUN J., NACEUR H., MORVAN H., DRAZETIC P., FONTAINE C., MAZERAN P.E., *Experimental characterization and micromechanical modeling of the elastic response of the human humerus under bending impact*, Mater. Sci. Eng., 2020, C 117, 111276.

[30] RHO J.Y., TSUI T.Y., PHARR G.M., *Elastic properties of human cortical and trabecular lamellar bone measured by nanoindentation*, Biomaterials, 1997, 18, 1325–1330.

[31] SAKAI M., SHIMIZU S., *Indentation rheometry for glass-forming materials*, J. Non-Crystalline Solids, 2001, 282, 236–247.

[32] SHIMIZU S., YANAGIMOTO T., SAKAI M., *Pyramidal indentation load–depth curve of viscoelastic materials*, J. Mater. Res., 1999, 14, 4075–4086.

[33] SMITH L.J., SCHIRER J.P., FAZZALARI N.L., *The role of mineral content in determining the micromechanical properties of discrete trabecular bone remodeling packets*, J. Biomech., 2010, 43, 3144–3149.

[34] STOCCHERO M., JINNO Y., TOIA M., JIMBO R., LEE C., YAMAGUCHI S., IMAZATO S., BECKTOR J.P., *In silico multi-scale analysis of remodeling peri-implant cortical bone: a comparison of two types of bone structures following an undersized and non-undersized technique*, J. Mech. Behav. Biomed. Mater., 2020, 103, 103598.

[35] TURNER C.H., WANG T., BURR D.B., *Shear Strength and Fatigue Properties of Human Cortical Bone Determined from Pure Shear Tests*, Calcif Tissue Int., 2001, 69 (6), 373–378.

[36] UNGER S., BLAUTH M., SCHMOELZ W., *Effects of three different preservation methods on the mechanical properties of human and bovine cortical bone*, Bone, 2010, 47, 1048–1053.

[37] WOFRAM U., WILKE H.-J., ZYSSET P.K., *Rehydration of vertebral trabecular bone: Influences on its anisotropy, its stiffness and the indentation work with a view to age, gender and vertebral level*, Bone, 2010, 46, 348–354.

[38] WU D., ISAKSSON P., FERGUSON S.J., PERSSON C., *Young's modulus of trabecular bone at the tissue level: A review*, Acta Biomater., 2018, 78, 1–12.

[39] ZLÁMAL P., JIROUŠEK O., KYTYR D., DOKTOR T., *Indirect determination of material model parameters for single trabecula based on nanoindentation and three-point bending test*, Eng. Mech., 2012, 1611–1620.

[40] ZYSSET P.K., *Indentation of bone tissue: a short review*, Osteoporos. Int., 2009, 20, 1049–1055.